A Novel Route to Toluene-Soluble Magnetic Oxide Nanoparticles: Aqueous Hydrolysis Followed by Surfactant Exchange

Moumita Ghosh,[‡] Gavin Lawes,[§] Arup Gayen,[‡] G. N. Subbanna,[⊥,†] W. M. Reiff,[#] M. A. Subramanian,[∥] A. P. Ramirez,[§] Jin-Ping Zhang,[▲] and Ram Seshadri*[,‡,▲]

Solid State and Structural Chemistry Unit, Indian Institute of Science, Bangalore 560 012, India, Los Alamos National Laboratories, Los Alamos, New Mexico, 87545, Materials Research Centre, Indian Institute of Science, Bangalore 560 012, India, DuPont Central Research and Development, Experimental Station, Wilmington, Delaware 19880, Department of Chemistry and Chemical Biology, Northeastern University, 102 Hurtig Hall, 360 Huntington Avenue, Boston, Massachusetts 02115, and Materials Department, University of California, Santa Barbara, California 93106-5050

Received July 17, 2003. Revised Manuscript Received October 20, 2003

The ability of capped nanoparticles of inorganic materials to dissolve in nonpolar solvents such as toluene creates opportunities for size-selective precipitation, surface modification through covalent means, incorporation into polymer composites, and the possibility of digestive ripening. Toluene-soluble nanoparticles are usually prepared in nonpolar solvents, where they are capped by hydrophobic surfactants; such preparations often require specialized high-temperature solvents and expensive precursors. Many transition metal oxides are easily prepared in nanoparticulate form cheaply and in quantity, by hydrolysis in aqueous media. However, capping of nanoparticles in aqueous media to make them nonpolar is usually difficult. We present here a simple process of *surfactant exchange* that permits ≈4-nm particles of the magnetic spinel oxides MFe_2O_4 (M = Mn and Zn) to be prepared in water in the presence of a surfactant and to then be transferred to toluene wherein the particles are capped by a second surfactant, a long-chain amine. The amine-capped nanoparticles can be successively precipitated and redissolved from their toluene solutions. Mössbauer spectroscopy and SQUID magnetization have been used to characterize magnetic properties of the nanoparticles.

Introduction

Capped nanoparticles of inorganic materials possess an inorganic core coated by a monolayer of an organic surfactant—the capping agent. Capping agents serve many purposes. They provide coordinative saturation of dangling bonds on the surface of the nanoparticle, thereby assisting in their stabilization. Entropic effects associated with long hydrocarbon chains discourage particles from approaching closely, and this further inhibits particle aggregation. In addition, when incorporated in the synthesis, capping agents can control particle size. Capping facilitates solubility and this opens up the possibility of size-selective precipitation,[1,2] a process which is at the heart of making monodisperse particles. Monodispersity in turn is essential to understanding the size-dependent properties of these materials and to forming nanocrystal superlattices.[3−5] Recently, Sorensen, Klabunde, and co-workers[6] showed that a process of "digestive ripening"—heating gold nanoparticle dispersions in solvents such as toluene in the presence of capping agents—can result in highly monodisperse nanoparticles even without size-selective precipitation. This work further underlines the importance of being able to dissolve nanoparticles in organic solvents.

Although capped nanoparticles of semiconductors[7,8] and metals[9] have been known for some years, reports

* To whom correspondence should be addressed. E-mail: seshadri@mrl.ucsb.edu. Fax: (805) 893 8797.
‡ Solid State and Structural Chemistry Unit, Indian Institute of Science.
§ Los Alamos National Laboratories.
⊥ Materials Research Centre, Indian Institute of Science.
∥ DuPont Central Research and Development.
Northeastern University.
▲ University of California.
† Deceased.

(1) Chemseddine, A.; Weller, H. *Ber. Bunsen-Ges. Phys. Chem.* **1993**, *97*, 636.
(2) Murray, C. B.; Norris, D. J.; Bawendi, M. G. *J. Am. Chem. Soc.* **1993**, *115*, 8706.
(3) Bentzon, M. D.; van Wonterghem, J.; Mørup, S.; Thölén, A. *Philos. Mag. B* **1989**, *60*, 169.
(4) Murray, C. B.; Kagan, C. R.; Bawendi, M. G. *Science* **1995**, *270*, 1335.
(5) Whetten, R. L.; Khoury, J. T.; Alvarez, M. M.; Murthy, S.; Vezmar, I.; Wang, Z. L.; Stephens, P. W.; Cleveland, C. L.; Luedtke, W. D.; Landman, U. *Adv. Mater.* **1996**, *8*, 428.
(6) Stoeva, S.; Klabunde, K. J.; Sorensen, C. M.; Dragieva, I. *J. Am. Chem. Soc.* **2002**, *124*, 2305. Prasad, B. L. V.; Stoeva, S. I.; Sorensen, C. M.; Klabunde, K. J. *Langmuir* **2002**, *18*, 7515.
(7) Fojtik, A.; Weller, H.; Koch, U.; Henglein, A. *Ber. Bunsen-Ges. Phys. Chem.* **1984**, *88*, 969.
(8) Steigerwald, M. L.; Alivisatos, A. P.; Gibson, J. M.; Harris, T. D.; Kortan, R.; Muller, A. J.; Thayer, A. M.; Duncan, T. M.; Douglas D. C.; Brus, L. E. *J. Am. Chem. Soc.* **1988**, *110*, 3046.
(9) Brust, M.; Walker, M.; Bethell, D.; Schiffrin, D. J.; Whyman, R. *J. Chem. Soc., Chem. Commun.* **1994**, 801.

10.1021/cm030346j CCC: $27.50
Published on Web 12/05/2003

on capping of oxide nanoparticles are sparse. Pileni and co-workers[10] have made extensive use of inverse micelles in a surfactant-as-reactant approach to prepare a number of spinel ferrite nanoparticles. In some of the cases, they used citrate ions to ensure dispersal in water. Sonochemical synthesis in the presence of long-chain surfactants has been used to make magnetic iron oxides.[11] Toluene-soluble oxide nanoparticles are a more recent innovation. Rockenberger, Scher, and Alivisatos[12] have prepared aliphatic amine-capped oxides by the thermolysis of cupferron precursors in trioctylamine. Such thermolysis can also be achieved solvothermally in toluene in the presence of amine-capping agents.[13] Recently, Rotello and co-workers[14] have demonstrated that long-chain amines do not bind very stably to oxide nanoparticle surfaces; long-chain 1,3 diols on the other hand bind stably and γ-Fe_2O_3 nanoparticles with 1,3-diol caps can be repeatedly precipitated from and redissolved in nonpolar solvents (unlike their amine-capped counterparts).

The preparation of toluene-soluble oxide nanoparticles (toluene being representative of a large class of nonpolar organic solvents) often calls for expensive, toxic high-temperature solvents such as trioctylamine[12] or triocylphosphine oxide (TOPO).[15] These solvents will not dissolve simple metal salts, and expensive metal sources (cupferronates, alkoxides, etc.) must be used. In addition, these solvents will not sustain hydrolysis, and instead thermolysis[12] or metathesis[15] is called for. Solvothermal techniques are one way to avoid expensive solvents and offer many possibilities for scale-up.[16]

Recently, we demonstrated that glycols can be used as inexpensive solvents in which the hydrolysis of simple Fe(III) salts in the presence of long-chain amines yield soluble, monodisperse nanoparticles.[17] Glycols are high boiling and sufficiently polar that they dissolve simple metal salts, and yet can incorporate long-chain amines. Glycols show great scope for scalable oxide nanoparticle preparations.[18,19] There have been some recent reports on capped, soluble, γ-Fe_2O_3 nanoparticles prepared by the decomposition of suitable precursors.[20]

The advantages of using water as the solvent, however, remain a strong attraction—apart from being "green", it becomes possible to use simple salts as the metal source. In addition, the reactions are cost-effective and therefore very amenable to scale-up. The problem with water is that it cannot solubilize any typical long-chain capping agent. In this contribution, we demonstrate that by a process of surfactant exchange, nanoparticles of the magnetic spinel oxides $MnFe_2O_4$ and $ZnFe_2O_4$ can be prepared in water in the presence of one surfactant and then transferred to a toluene solution of another surfactant, where they are more strongly capped. The first surfactant is cetyl trimethylammonium bromide (CTAB), which readily disperses in water. In toluene, the surfactant used is *n*-octylamine.

Our method is inspired by the phase transfer route of Brust et al.[9] for the preparation of Au nanoparticles and also by work from Rao and co-workers showing that noble metal nanoparticles can be transferred from water to toluene simply by decreasing the pH of the aqueous phase.[21] Gittins and Caruso[22] have demonstrated the opposite process by transferring palladium nanoparticles from a toluene solution to water through exchange of capping agent.

Experimental Section

To prepare ≈4-nm $ZnFe_2O_4$ nanoparticles, 100 cm^3 of 0.2 M aqueous solution of $FeCl_3 \cdot 6H_2O$ was mixed with 100 cm^3 of 0.1 M aqueous solution of $ZnCl_2 \cdot 4H_2O$ in a 500-cm^3 beaker. To prepare $MnFe_2O_4$ nanoparticles, $MnCl_2 \cdot 4H_2O$ was taken instead of $ZnCl_2 \cdot 4H_2O$. The solution was heated to 70 °C. Then 50 cm^3 of a 0.3 M aqueous solution of cetyl trimethylammonium bromide (CTAB) was added and heating was continued. A hot aqueous solution of 3 M NaOH at the same temperature was then added to reach the desired pH (typically pH = 12). The contents of the beaker were continuously stirred with a magnetic Teflon-coated stir bar during the course of the reaction. Except for the addition of CTAB, the procedure closely follows Sato et al.[23] for the preparation of $ZnFe_2O_4$ nanoparticles and that of Kang et al.[24] for spinel Fe_3O_4 nanoparticles starting from Fe(II) and Fe(III) chlorides. After holding at the reaction temperature for 1 h, the contents were allowed to cool to room temperature whereupon a brown ($ZnFe_2O_4$) or grayish-black ($MnFe_2O_4$) product precipitated. Precipitation was greatly facilitated by placing a strong magnet below the beaker. Collection of solid material was achieved by decanting the clear supernatant liquid.

The solid material was washed in water to remove any starting material or salt (NaCl, formed during the hydrolysis). The material was then dried in a hot air oven at 40 °C for 24 h to obtain the crude product. When 1 g of the crude product was taken in 50-cm^3 toluene and sonicated in a bath sonicator, no change in the color of liquid was noted and the solid remained in particulate form. However, upon addition of 3−4 cm^3 of *n*-octylamine before the sonication, a change of solution color was observed. After 12 h, the color of the solution was wine red. From this wine red solution, solid material could be reprecipitated by addition of 2-propanol. All further characterization was performed on the reprecipitated material, after washing it extensively with 2-propanol to remove any physisorbed organic matter.

The reprecipitated material easily dissolves in toluene, provided some *n*-octylamine is added (about 5 vol %).[17] The need for an excess of capping agent is indicative of the rather ineffectual binding of amine to the oxide surface.[14]

If the crude product from the aqueous reaction is first washed with an organic solvent such as acetone or 2-propanol,

(10) Pileni, M. P. *Langmuir* **1997**, *13*, 3266.
(11) Kataby, G.; Prozorov, T.; Koltypin, Yu.; Cohen, H.; Sukenik, C. N.; Ulman, A.; Gedanken, A. *Langmuir* **1997**, *13*, 6151.
(12) Rockenberger, J.; Scher, E. C.; Alivisatos, A. P. *J. Am. Chem. Soc.* **1999**, *121*, 11595.
(13) Thimmaiah, S.; Rajamathi, M.; Singh, N.; Bera, P.; Meldrum, F. C.; Chandrasekhar, N.; Seshadri, R. *J. Mater. Chem.* **2001**, *11*, 3215.
(14) Boal, A. K.; Das, K.; Gray, M.; Rotello, V. M. *Chem. Mater.* **2002**, *14*, 2628.
(15) Trentler, T. J.; Denler, T. E.; Bertone, J. F.; Agrawal, A.; Colvin, V. L. *J. Am. Chem. Soc.* **1999**, *121*, 1613.
(16) Rajamathi, M.; Seshadri, R. *Curr. Opin. Solid State Mater. Sci.* **2002**, *6*, 337.
(17) Rajamathi, M.; Ghosh, M.; Seshadri, R. *J. Chem. Soc., Chem. Commun.* **2002**, 1152.
(18) Ammar, S.; Helfen, A.; Jouini, N.; Fiévet, F.; Rosenman, I.; Villain, F.; Molinié, P.; Danot, M. *J. Mater. Chem.* **2001**, *11*, 186.
(19) Carunto, D.; Remond, Y.; Chou, N. H.; Jun, M.-J.; Carunto, G.; He, J.; Goloverda, G.; O'Connor, C.; Kolenichenko, V. *Inorg. Chem.* **2002**, *41*, 6137.
(20) Hyeon, T.; Lee, S. S.; Park, J.; Chung, Y.; Na, H. B. *J. Am. Chem. Soc.* **2001**, *123*, 12798. Bourlinos, A. B.; Simopoulos, A.; Petridis, D. *Chem. Mater.* **2002**, *14*, 899. Bourlinos, A. B.; Bakandritsos, A.; Georgakilas, V.; Petridis, D. *Chem. Mater.* **2002**, *14*, 3226. Sun, S.; Zeng. H. J. *Am. Chem. Soc.* **2002**, *124*, 8204.
(21) Vijaya Sarathy, K.; Kulkarni, G. U.; Rao, C. N. R. *J. Chem. Soc. Chem. Commun.* **1997**, 537.
(22) Gittins, D. I.; Caruso, F. *Angew. Chem., Int. Ed.* **2001**, *40*, 3001.
(23) Sato, T.; Haneda, K.; Seki, M.; Iijima, T. *Appl. Phys., A* **1990**, *50*, 13.
(24) Kang, Y. S.; Risbud, S.; Rabolt, J. F.; Stroeve, P. *Chem. Mater.* **1996**, *8*, 2209.

CTAB adhering to the solid mass is removed. It is then not possible to dissolve the nanoparticles in toluene/*n*-octylamine solutions. This suggests that while binding of CTAB to the nanoparticles is weak, in its absence, the nanoparticles aggregate too strongly to be dispersed.

By controlling the pH (between 8 and 13) and temperature (between 40 and 100 °C), we were able to prepare toluene-soluble $ZnFe_2O_4$ and $MnFe_2O_4$ nanoparticles of different sizes (as monitored by X-ray diffraction line broadening) in gram quantities. However, we restrict our attention here to a detailed study of the ≈4-nm particles of the two materials. Control over size in hydrolytic preparations of spinel oxide particles has been described in detail by Sato et al.[23]

Powder XRD patterns were acquired in the $\theta-2\theta$ Bragg–Brentano geometry on a Siemens D5005 diffractometer using Cu Kα radiation with a scan rate of 1° 2θ per minute. The data were then rebinned into 0.10° steps. Samples were prepared for transmission electron microscopy (TEM) by placing a drop of toluene solution of the nanoparticles on carbon-coated Cu TEM grids, letting excess solvent drain away. The grids were examined using a JEOL 2010 high-resolution electron microscope operating at 200 kV with a point-to-point resolution better than 2 Å (as calibrated using the 200 lattice spacing of gold). Energy-dispersive X-ray (EDX) analysis of the nanoparticles made use of a Link ISIS system attached to a JEOL JSM 5600LV scanning electron microscope. Core level X-ray photoelectron spectra (XPS) of the nanoparticles were recorded using Al Kα incident X-rays on a Vaccuum Generators ESCA 3 Mk II instrument operated at a vacuum of better than 2×10^{-10} Torr. Pressed pellets of the samples were subject to magnetic measurement using a Quantum Design SQUID magnetometer.

Mössbauer spectra were acquired using a conventional constant acceleration spectrometer operated in multichannel scaling mode. The γ-ray source (DuPont-Merck Co.) consisted of 51.5 mCi of Co^{57} in a rhodium metal matrix that was maintained at ambient temperature. The spectrometer was calibrated using a 6-μm-thick natural abundance iron foil. Isomer shifts are reported relative to the center of the magnetic hyperfine pattern of the latter foil taken as zero velocity. The line widths of the innermost pair of $\Delta M_I = \pm 1$ transitions of the latter Zeeman pattern were reproducibly determined to be 0.214 mm/s. Sample temperature variation was achieved using a standard exchange gas liquid helium cryostat (Cryo Industries of America, Inc.) with temperature measurement and control based on silicon diode thermometry in conjunction with a 10-μA excitation source (Lakeshore Cryotronics, Inc). Spectra were fit to unconstrained Lorentzians using the program ORIGIN (Originlab Corporation).

Results and Discussion

$ZnFe_2O_4$. To characterize phase purity of the nanoparticles, as well as obtain estimates of particle sizes, step-scanned powder XRD patterns of reprecipitated, *n*-octylamine-capped $ZnFe_2O_4$ particles were subject to Rietveld refinement using the XND Rietveld code.[25] For the refinement, the scale factor, profile parameters, and the cubic cell parameter were freed. The XRD pattern refined in the spinel structure with a cell parameter of 8.46(1) Å. The resulting fit is displayed in Figure 1. The refinement permitted deconvolution of the 311 peak at 35.16° 2θ. The width was used to determine particle size from the Scherrer formula. The particles were found to possess a mean size of 3.5 nm. The TEM image of the particles dispersed from solution on a carbon-coated Cu grid is displayed in Figure 2. The particles are seen to be rather isotropic, and in high resolution (shown in the inset) are seen to be quite crystalline. The lattice planes

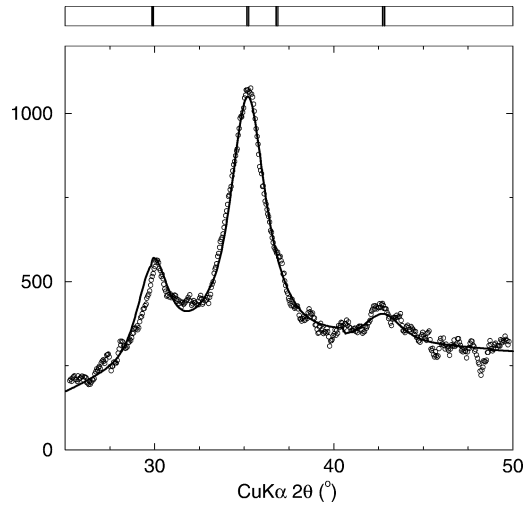

Figure 1. Powder XRD pattern of *n*-octylamine-capped $ZnFe_2O_4$ nanoparticles showing data (points) and the Rietveld fit (solid line). Vertical lines at the top of the figure are expected peak positions for the cubic spinel structure.

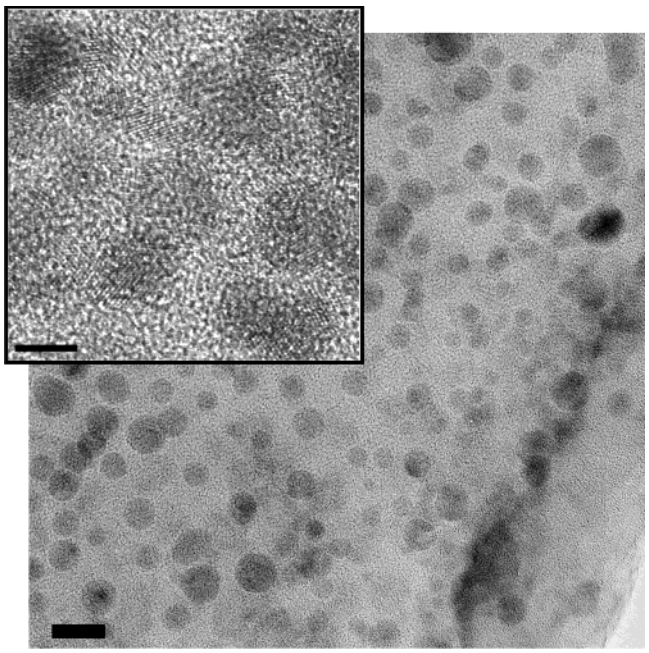

Figure 2. TEM image of *n*-octylamine-capped $ZnFe_2O_4$ nanoparticles. The bar corresponds to 10 nm. The inset is a high-resolution image of a few particles (bar = 3 nm).

of some particles are imaged in the inset of Figure 2. The mean diameter was determined to be 4.5 nm with a standard deviation of 1.0 nm. The discrepancy between the XRD and TEM estimates of the particle size could arise from the particles being twinned—the TEM estimate and the XRD estimate would be similar only if the particles were all single crystals. Indeed, the TEM image in the inset of Figure 2 indicates that, for some particles, the directions of the lattice planes are not the same through the entire particle. Poor crystallinity of the particles could be a consequence of the low temperature of preparation. In our previous studies on spinel nanoparticles made at higher temperatures (greater than 200 °C in solvothermal toluene)[13] than used in this study, TEM and XRD provided similar estimates of particle size.

(25) Bérar, J.-F.; Garnier, P. *NIST Spec. Publ.* **1992**, *846*, 212.

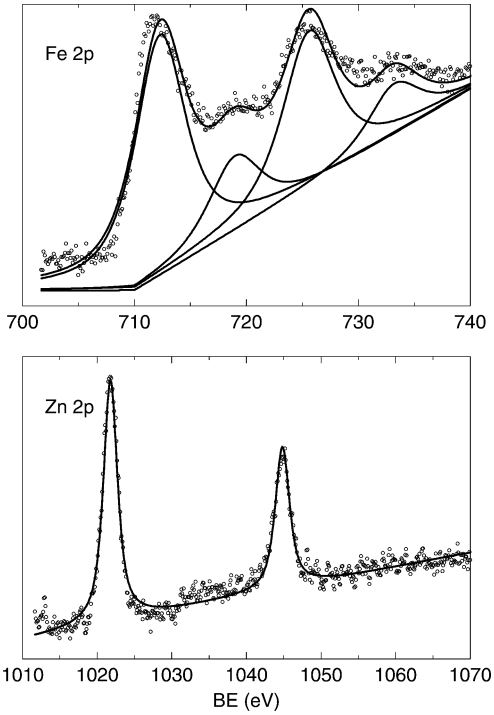

Figure 3. Fe 2p and Zn 2p core-level X-ray photoelectron spectra of the $ZnFe_2O_4$ nanoparticles. Deconvolution of the spectra into Lorentzians is shown. The peaks are split into $2p_{1/2}$ and $2p_{3/2}$. In addition, the Fe 2p spectrum displays satellites for each of these peaks.

The two panels of Figure 3 show core level XPS of $ZnFe_2O_4$ particles in the Fe 2p and Zn 2p regions of the binding energy. In the Fe 2p spectrum, the two major components (at 712 and 726 eV) arise from $2p_{3/2}$ and $2p_{1/2}$ contributions, and each of these have a satellite. The energies and the presence of satellites are consistent with Fe^{III}.[26] In the Zn spectrum, there are no satellites because of the d^{10} configuration. From an integration of areas under the peaks, a ratio of Zn:Fe of 0.59 is obtained using standard formuli.[26] This is close to the expected ratio of 0.5 for spinel $ZnFe_2O_4$ and justifies our assignment of the formula. We note that neither XPS nor powder XRD are able to provide us with details of site selection: the extent of inversion of Fe ions into the Zn site of the structure and vice versa.

To establish surfactant exchange, from a relatively weakly bound coating of CTAB on the crude product, to a more strongly bound coating of the amine, we have examined the crude and reprecipitated products by FT-IR spectroscopy and by EDX analysis. Panel (a) of Figure 4 displays FT-IR spectra of the crude product (solid line) and reprecipitated product (dashed line) in the CH stretch region around 2900 cm^{-1}. Peaks in the IR spectrum of the crude product are significantly broader than those in the spectrum of the reprecipitated product. In the CTAB-coated particles, the surfactant is only physisorbed, and the hydrocarbon chains are disordered, resulting in a broad CH stretch signal. In the reprecipitated product, on which *n*-octylamine chains are better bound, one expects greater coherence in the CH_2 groups in the chain, and hence the sharper CH stretch signal.

More direct evidence for the presence of CTAB on the surface of the crude material is seen in the EDX spectrum (solid line) in Figure 4b, where Br L-edge

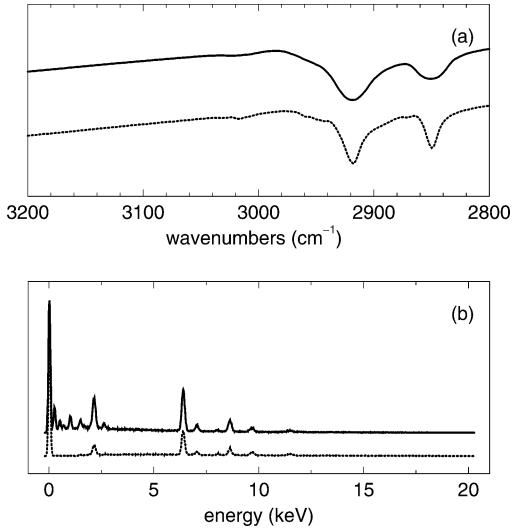

Figure 4. (a) FT-IR spectra in the CH stretch region for the crude $ZnFe_2O_4$ nanoparticles (solid line) and the reprecipitated nanoparticles (dotted line). (b) EDX spectra for the crude (solid) and reprecipitated (dotted) nanoparticles.

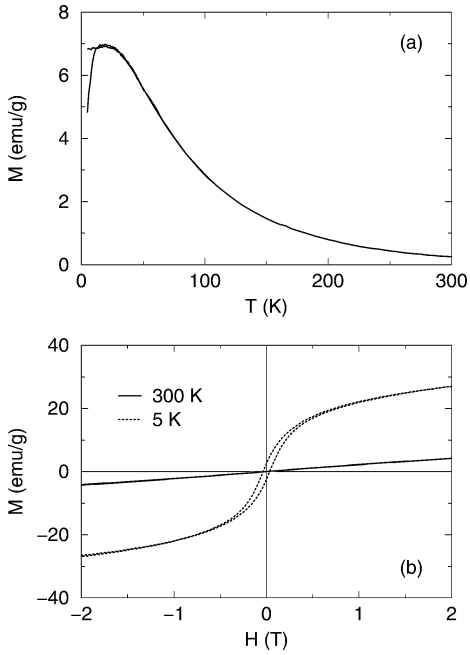

Figure 5. (a) Magnetization as a function of temperature for a pressed pellet of the $ZnFe_2O_4$ nanoparticles. The data were acquired under a 1000 Oe field, after field cooling and cooling under zero field. (b) *M* vs *H* at 300 and 5 K.

X-rays in the energy region between 0 and 2 keV are clearly observed, along with the K-edge X-rays of Fe (7.1 keV) and K-edge X-rays of Zn (9.6 keV). For the reprecipitated, amine-capped nanoparticles (dashed line), X-ray signals in the Br L-edge energy region are missing.

Pressed pellets of the 4-nm $ZnFe_2O_4$ nanoparticles were examined by SQUID magnetometry. Figure 5a displays the *M* vs *T* trace acquired after zero field cooling (ZFC) and field cooling (FC) under a 1000 Oe field. At low temperatures (below $\approx$ 12 K), separation of the FC and ZFC traces is observed. $ZnFe_2O_4$ is a weak

(26) Briggs, D.; Seah, M. P. *Practical Surface Analysis by Auger and X-ray Photoelectron Spectroscopy*, 2nd ed.; John Wiley and Sons: New York, 1990.

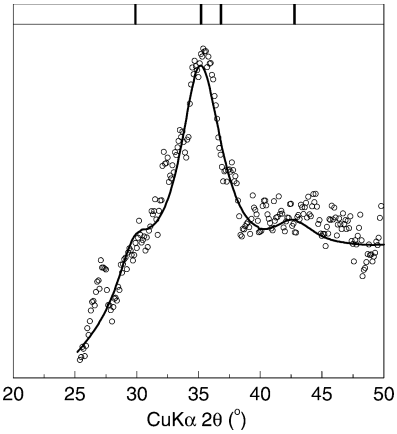

Figure 6. Powder XRD pattern of $MnFe_2O_4$ nanoparticles showing data (points) and the Rietveld fit (solid line). Vertical lines at the top of the figure are expected peak positions for the cubic spinel structure.

ferrimagnet, with the principal interaction being antiferromagnetic exchange between octahedral Fe^{III} and Fe ions (both divalent and trivalent) that are exchanged into the tetrahedral Zn site of the spinel structure. The magnetism therefore critically depends on the ordering of ions (site selection). In addition, the very small size of the particles would further weaken magnetism. Divergence of the FC and ZFC traces takes place below about 12 K, suggesting blocking of superparamagnetism below this temperature. The data are fully consistent with the material comprising nanoparticles of a rather soft magnetic material. Plots of M vs H recorded at temperatures of 300 and 5 K are displayed in the two panels of Figure 5b. At 300 K, the particles do not display saturation behavior, and only very weak collective behavior (in the deviation from linearity). At 5 K, weak hysteresis becomes evident with a coercivity of 360 Oe and a saturation magnetization M_s near 28 emu g^{-1}. As the magnetic properties of spinel (particularly $ZnFe_2O_4$) particles depend crucially on site selection, which in turn is influenced by the method of preparation, comparing magnetism across samples prepared by different means is difficult. However, rather similar behavior to what is found here has been reported by Pileni and co-workers for ≈3-nm $ZnFe_2O_4$ nanoparticles[27] prepared by an oil-in-water emulsion route: both in the nature of the low-temperature hysteresis loop, as well as values of coercivity and saturation magnetization. The unusually strong downturn in the ZFC magnetization at low temperatures— a characteristic associated with antiferromagnetic than ferrimagnetic materials—has also been noted by these authors.

$MnFe_2O_4$. Rietveld refinement of step-scanned powder XRD pattern of the reprecipitated octylamine-capped $MnFe_2O_4$ particles (Figure 6) yielded a cubic cell parameter of 8.46(3) Å and an average particle size (from deconvolution of the 311 peak) of 2.3 nm. The TEM image of these particles is displayed in Figure 7. The edges of these particles are less well defined, but are consistent with a size of about 3 nm. In the high-resolution images (inset) lattice planes of the spinel crystal are visible for some particles.

(27) Hochepied, J. F.; Bonville, P.; Pileni, M. P. *J. Phys. Chem. B* **2000**, *104*, 905.

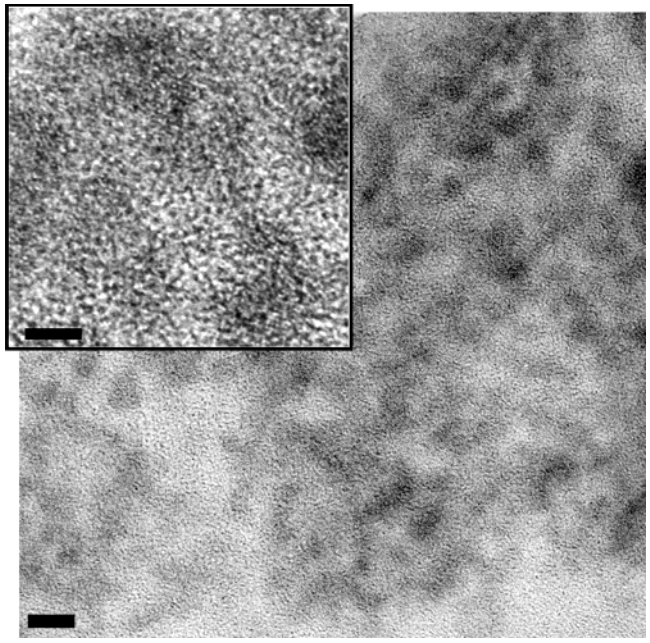

Figure 7. TEM micrograph of $MnFe_2O_4$ nanoparticles. The bar corresponds to 10 nm. The inset shows a few particles at higher magnification (bar = 5 nm).

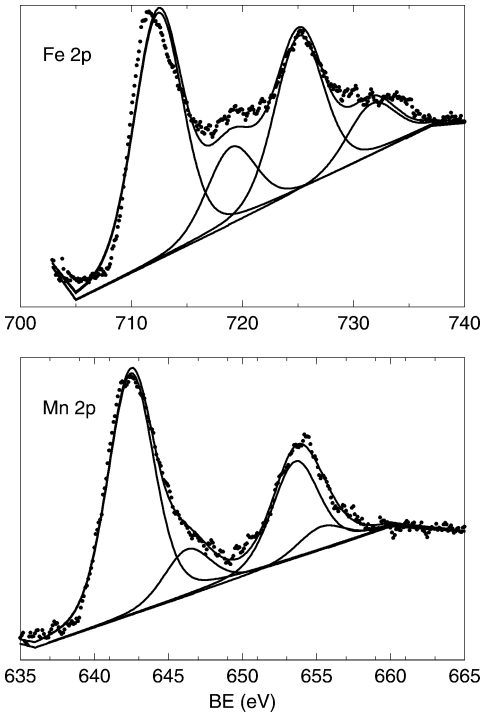

Figure 8. Fe 2p and Mn 2p core-level X-ray photoelectron spectra of the $MnFe_2O_4$ nanoparticles. Deconvolution of the spectra into Lorentzians is shown. The peaks are split into $2p_{1/2}$ and $2p_{3/2}$, with corresponding satellites.

Core level XP spectra of the $MnFe_2O_4$ sample shown in Figure 8 are consistent with an Mn:Fe ratio of 0.50 and average oxidation states of 2+ for Mn and 3+ for Fe.

Figure 9a shows the M vs T traces for a pressed pellet of the $MnFe_2O_4$ nanoparticles under different fields of 10, 50, 500, and 1000 Oe (a−d). For the 1000 Oe measurement, both ZFC and FC traces are displayed, and these are found to separate below ≈27 K. The divergence of FC and ZFC traces in the 1000 Oe

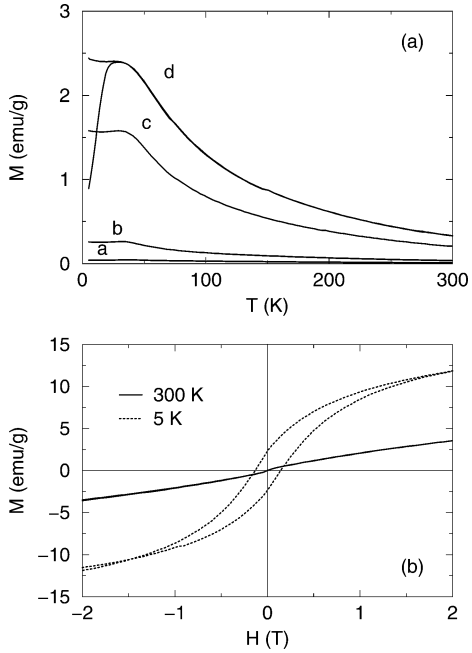

Figure 9. (a) Magnetization as a function of temperature for a pressed pellet of the $MnFe_2O_4$ nanoparticles. a, b, c, and d indicate data acquired under fields of 10, 50, 500, and 1000 Oe. For the 1000 Oe run, field cooled and zero field cooled data are shown. (b) *M* vs *H* at 300 and 5 K.

measurement suggests a blocking temperature near 27 K. Plots of *M* vs *H* acquired at 300 K and at 5 K [Figure 9b] confirm weak superparamagnetism and the blocking. The 5 K data indicate a saturation magnetization near 13 emu g^{-1} and a rather large coercivity of 1350 Oe—in fact, coercivity is known to increase with decreasing particle size.[27] Chen et al.[28] have made an extensive study of size dependence of the magnetic properties of precipitated $MnFe_2O_4$ particles in the 5−15-nm size regime, including an examination of the influence of cation site selection. Extrapolating their plots of saturation magnetization as a function of inverse diameter suggests that, for ≈3-nm particles, the value should approach 20 emu g^{-1}. This is larger than the value observed here. This suggests either that the linear relation of M_s with inverse diameter does not extend to very small particles or that we have not properly accounted for the amount of capping agent on the particles. If the mass of magnetic ions were more precisely known, M_s determined here might be closer to the values suggested by these authors. Liu and Zhang[29] have prepared $MnFe_2O_4$ nanoparticles using inverse-micelle routes, with sizes ranging from 4 to 14 nm. For 4.4-nm particles, they find a saturation magnetization of 30 emu g^{-1} at 20 K.

Mössbauer Studies. The temperature dependencies of the zero field Mössbauer spectra of $MnFe_2O_4$ and $ZnFe_2O_4$ are shown in the different panels of Figure 10. The limiting low-temperature spectra of both ferrites exhibit clear asymmetric broadening of transitions 1 and 6 of their Zeeman patterns.[30] This behavior is typical and has been previously associated with partial inversion in the small particle size (nanometric) forms of these materials relative to the (essentially) normal spinel bulk form known for the Mn and Zn analogues.[31] The enhanced tetrahedral A site Fe^{3+} population corresponding to inversion is generally not resolved in zero field Mössbauer spectra.[32] In any event, the present Mössbauer spectra provide additional definitive microscopic evidence that the synthetic approach discussed herein affords genuine significantly inverted nanoscale particles. In particular, the general form of the spectral temperature dependence is that of onset of slow (superparamagnetic) relaxation below ≈80 K while the total collapse of the internal field normally observed for $MnFe_2O_4$ at ambient temperature is consistent with particle size certainly below 10 nm.[33] (Bulk $MnFe_2O_4$ is fully hyperfine split corresponding to an average internal field for the A and B sites ≈46 T[34]). In the present study, the internal hyperfine fields for the $MnFe_2O_4$ and $ZnFe_2O_4$ are 48.1 and 48.6 T, respectively, at 4.2 K, suggesting that neither material is fully magnetically saturated on the Mössbauer spectroscopy time scale in zero field. At saturation and including small covalency reduction effects of the hyperfine fields, one would have expected internal fields of the order of

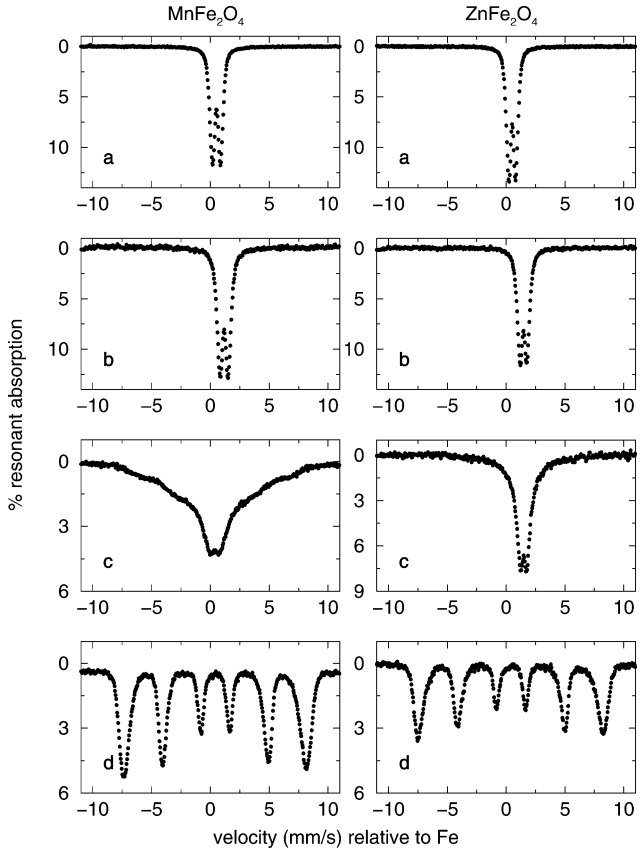

Figure 10. Temperature dependence of the zero field Mössbauer spectra of the $MnFe_2O_4$ (left panels) and $ZnFe_2O_4$ (right panels) nanoparticles. The temperatures are (a) 293 K, (b) 77.5 K, (c) 48.5 K, and (d) 4.2 K.

(28) Chen, J. P.; Sorensen, C. M.; Klabunde, K. J.; Hadjipanayis, G. C.; Devlin, E.; Kostikas, A. *Phys. Rev. B* **1996**, *54*, 9288.
(29) Liu, C.; Zhang, Z. *J. Chem. Mater.* **2001**, *13*, 2092.
(30) Ahn, Y.; Choi, E. J.; Kim, S.; An, D. H.; Kang, K. U.; Lee, B. G.; Baek, K. S.; Oak, H. N. *J. Korean Phys. Soc.* **2002**, *41*, 123.
(31) Greenwood, N. N.; Gibb, T. C. *Mössbauer Spectroscopy*; Chapman and Hall Ltd.: London, 1971.
(32) Mahmoud, M. H.; Hamdeh, H. H.; Ho, J. C.; O'Shea, M. J.; Walker, J. C. *J. Magn. Magn. Mater.* **2000**, *220*, 139.
(33) Kundig, W.; Bömmel, H.; Constabaris, G.; Lindquist, R. H. *Phys. Rev.* **1966**, *142*, 327.
(34) Sawatzky, G. A.; Van Der Woude, F.; Morrish, A. H. *Phys. Lett.* **1987**, *25A*, 147.

50 T or slightly greater.[31] Finally, a previous detailed Mössbauer spectroscopy study[30] of nanoparticles (9 nm) of $ZnFe_2O_4$ shows a spectrum at 52 K that exhibits partial magnetic hyperfine spitting. (This spectrum is generally similar to ours for $MnFe_2O_4$ at 48.5 K.) Our spectrum of $ZnFe_2O_4$ exhibits only incipient broadening/"wing-like" behavior at 48.5 K consistent with its substantially smaller particle size, of about 3 versus 9 nm.

Conclusions

We have demonstrated that a simple and inexpensive process of hydrolysis in water can be employed to prepare toluene-soluble spinel oxide nanoparticles through a process of surfactant exchange. The use of water as a solvent means that simple salts can be used as the metal source and that the reaction is easily amenable to scale-up. The ability of the nanoparticles to dissolve in toluene opens up the possibility of size-selective precipitation, digestive ripening, modification of surface chemistry, and incorporation into organic matrixes such as polymers. While our demonstration has focused on ≈4-nm particles of $ZnFe_2O_4$ and $MnFe_2O_4$, the technique can easily be extended to other spinel ferrites as well and to particles of different sizes.

Acknowledgment. M.G. and R.S. have been supported by the Department of Science and Technology, India. We thank Professor M. S. Hegde for placing XPS facilities at our disposal. This work made use of MRL (UCSB) Central Facilities supported by the National Science Foundation under Award No. DMR 96-32716.

CM030346J